*metals*

MDPI

*Article*

# Synergistic Effect of RE (La, Er, Y, Ce) and Al-5Ti-B on the Microstructure and Mechanical Properties of 6111Aluminum Alloy

**Chuanchao Meng [1], Changchao Su [1], Zhenkuan Liu [1], Dongxing Liao [1], Xincheng Rong [1], Yuanzhuo Li [1], Hongqun Tang [1,2,*] and Junsheng Wang [3,4,*]**

[1] State Key Laboratory of Featured Metal Materials and Life-Cycle Safety for Composite Structures, School of Resources, Environment and Materials, Guangxi University, Nanning 530004, China
[2] Key Laboratory of High-Performance Structural Materials and Thermo-Surface Processing, Education Department of Guangxi Zhuang Autonomous Region, Guangxi University, Nanning 530004, China
[3] School of Materials Science and Engineering, Beijing Institute of Technology, Beijing 100081, China
[4] Advanced Research Institute of Multidisciplinary Science, Beijing Institute of Technology, Beijing 100081, China
* Correspondence: hqtang@gxu.edu.cn (H.T.); junsheng.wang@bit.edu.cn (J.W.)

**Abstract:** For aluminum alloys, grain refinement is one of the effective methods for improving both strength and ductility. However, the refining effect of Al-Ti-B master alloy refiners deteriorates due to the agglomeration and sinking of the second phase particles. In this paper, the effects of rare earth type, rare earth content, and holding time on the microstructure and properties of Al-5Ti-B + RE/6111 were investigated by orthogonal experiment. It was shown that the addition of rare earth promoted the transformation of the β-$Al_5FeSi$ phase to an α-$Al_{15}(Mn,Fe)_3Si_2$ phase, while the segregation of rare earth made it difficult for $TiB_2$ to aggregate and inhibited the growth of $TiAl_3$, resulting in more particles becoming effective nucleation substrates. The Al-5Ti-B + Ce master alloy developed based on orthogonal experiment improved the refinement recession problem well and improved the comprehensive mechanical properties of 6111 aluminum alloy. It was found that the addition of Al-5Ti-B + 0.1Ce, which had an ultimate tensile strength of 240.4 ± 2.2 MPa, successfully reduced the grain size by 73.8% and improved elongation by 37.8% compared to the base alloy. There search is of great significance for the preparation and application of high-performance rare earth 6111 aluminum alloy.

**Keywords:** 6111aluminum alloy; grain refiner; Al-Ti-B master alloy; rare earth; refining mechanism

check for updates

**Citation:** Meng, C.; Su, C.; Liu, Z.; Liao, D.; Rong, X.; Li, Y.; Tang, H.; Wang, J. Synergistic Effect of RE (La, Er, Y, Ce) and Al-5Ti-B on the Microstructure and Mechanical Properties of 6111Aluminum Alloy. *Metals* **2023**, *13*, 606. https://doi.org/10.3390/met13030606

Academic Editor: Noé Cheung

Received: 30 December 2022
Revised: 7 March 2023
Accepted: 9 March 2023
Published: 16 March 2023

**Copyright:** © 2023 by the authors. Licensee MDPI, Basel, Switzerland. This article is an open access article distributed under the terms and conditions of the Creative Commons Attribution (CC BY) license (https://creativecommons.org/licenses/by/4.0/).

## 1. Introduction

Aluminum alloys are widely used in the transport industry, medical equipment, and construction materials due to their abundant resources, lightweight, good mechanical properties, good corrosion resistance, and good electrical conductivity [1]. With carbon neutrality becoming a global consensus, the light-weighting of machinery and equipment, especially automobiles, has become an important direction for future development [2]. Aluminum alloy, which is the main material for the light-weighting of cars, is prone to forming coarse grain, which is not conducive to its strength and plasticity, limiting its application in key components [3]. Over the past few decades, various techniques have been used to improve the strength and elasticity of aluminum alloys. Grain refinement is an effective method for simultaneously enhancing the strength and plasticity of aluminum alloys. The addition of master alloys containing refiners to control the nucleation and growth of α-Al grains during solidification has become a standard practice in the aluminum casting industry [4]. At the same time, the increase of grains not only reduces defects, such as segregation and porosity in castings, but it also eliminates columnar structure, thus improving the quality of wrought aluminum alloys by improving formability [5,6]. The most widely used master alloy refiner has been the Al-Ti-B grain refiner [7]. However,

the Al-Ti-B master alloy refiner has easy recession [8], silicon poisoning [9], zirconium poisoning [10], and other problems, and has not been able to meet the needs of high-performance aluminum alloy production. Therefore, in recent years, many researchers have continued to explore its recession [11] and poisoning mechanism [12] and have tried to develop new anti-recession [8] anti-poisoning [13–15] master alloy refiners.

In the industrial production of aluminum alloys, if the melt is not cast directly but left to stand for a long time after the addition of master alloys, a coarse grain is obtained instead of fine equiaxed crystals, which is a phenomenon known as refinement "recession". This is very common in the production of aluminum alloys, making the refinement effect of the master alloy significantly weaker and getting a columnar crystal or feather crystal, which is attributed to the aggregation, precipitation, or decomposition of particles in the master alloy [16] Research on the master alloy refiner of aluminum alloy started late in China and was initially to block Al-Ti-B into the aluminum melt, although it also played a role in the refining effect of aluminum alloy grain; however, this method of addition makes the second phase particle high density, and easy to gather precipitation when at rest, and thus, the phenomenon of refinement declined. Later, a technology developed in the USA was introduced to continuously add filamentary Al-Ti-B to the flow bath melt using automated equipment, which effectively alleviated the aggregation and precipitation of the second phase particles. But more was needed to fundamentally solve the problem of refinement recession. The recession of the aluminum melt after adding Al-Ti-B was mainly due to the aggregation of $TiAl_3$ and $TiB_2$ particles. Mohanty et al. [17] studied the aggregation of particles after standing using a metal purity analyzer. They added Al-5Ti-B to the aluminum melt, treated it for 5 min, and then stirred it uniformly. 0.063 wt.% Ti and 0.012 wt.% B were analyzed at the bottom, and 0.306% Ti and 0.114% B were analyzed at the bottom after one day of standing.

The grain size and morphology of $TiAl_3$ and $TiB_2$ phases have an important effect on the grain refining efficiency of Al-Ti-B master alloys [18]. Attempts have been made to grind grains by mechanical agitation, magnetohydrodynamic mixing, or ultrasonic grinding [19]. These methods have achieved some results, but they cannot completely replace Al-Ti-B. Al-Ti-B-RE is considered to be a very promising anti-recession refiner. The Beijing Institute of Technology [20], the Lanzhou University of Technology [21], and some other institution shave studied the refining properties of rare earth Al-Ti-B master alloys and found that rare earth Al-Ti-B master alloys have a good effect on the microstructure and properties of the base. Ma et al. [22] found that the decomposition of TiAlEr compounds, which released Er, refrained the growth of $TiAl_3$ and made $TiB_2$ difficult to aggregate or deposit; therefore, this resulted in more particles being efficient nucleation substrates. Chen et al. [23] found that rare earth can reduce the size and surface energy of the $TiB_2$phase by adsorption onto the surface of $TiB_2$phase, thus reducing the possibility of agglomeration. However, due to the varieties of rare earth and their very active nature, the related research was not systematic enough and the products were not mature and stable enough; specifically, the anti-recession mechanism of Al-Ti-B-RE master alloys and the interaction between rare earth and Al-Ti-B have not been studied systematically.

In this study, the effects of varieties of rare earth, the content of rare earth, and holding time on the grain size and the mechanical properties of Al-5Ti-B + RE/6111 were investigated using orthogonal experiment. The effects of rare earth on the Al-5Ti-B master alloy and the microstructure and properties of 6111 base were investigated thermodynamically and experimentally, and the mechanisms were analyzed. This study provides some implications for the development of high-performance 6111 aluminum alloys.

## 2. Materials and Methods

### *2.1. Sample Preparation*

In this paper, the refinement effects of Al-5Ti-B, Al-5Ti-B + La, Al-5Ti-B + Er, Al-5Ti-B + Y, and Al-5Ti-B + Ce master alloy refiners were investigated in a 6111 casting process. Table 1 shows the details of the orthogonal experiment; combining rare earth types, rare earth

content, and holding time were listed as the three factors in the orthogonal experiment, with four levels of each factor. The base was named No. 1, and No. 2 was supplemented with 0.6% Al-5Ti-B. No.'s 3 to 6 were supplemented with Al-5Ti-B + La, No.'s 7 to 10 with Al-5Ti-B + Er, No.'s 11 to 14 with Al-5Ti-B + Y, and No.'s 15 to 18 withAl-5Ti-B + Ce.

**Table 1.** Details of the orthogonal experiment.

| Level | Rare Earth Types A | Rare Earth Content (wt.%) B | Holding Time (min) C |
|---|---|---|---|
| 1 | La | 0.1% | 5 min |
| 2 | Er | 0.2% | 10 min |
| 3 | Y | 0.3% | 15 min |
| 4 | Ce | 0.4% | 20 min |

Before each casting, 100 g of raw material was prepared, mechanically polished, and cleaned in an alcohol-filled ultrasonic shaking bath to remove surface impurities and oxides. After treating the surfaces, all samples and melting tools, such as graphite rods and molds, were preheated in an oven at 250 °C for 20 min to ensure the experiment's safety and reduce the introduction of hydrogen into the melt. Firstly, 6111 was melted in a high-temperature melting furnace at 750 °C, stirred with 0.5% refining agent (NaCl:KCl = 1:1) and 0.3% degassing agent ($C_2Cl_6$), and held for 10 min before slagging. The melt was then cleaned and the corresponding master alloy was added according to the orthogonal experiment table and stirred and held for the corresponding time, as shown in Table 2. Finally, the No.1 sample was poured into the steel mold, and the other sample alloys were poured into the copper mold to cool and solidify. After casting into ingots, the specimens were cut into 15 mm × 15 mm × 5 mm metallographic samples and tensile samples with a maximum length of 82 mm. The experimental procedure is shown in Figure 1. The master alloys were prepared similarly. After Al-5Ti-B was refined and de-gassed, Al-10RE was added to obtain the corresponding Al-5Ti-B + RE master alloy.

**Table 2.** Orthogonal experiment scheme and experimental results.

| Alloy Number | Rare Earth Types | Rare Earth Content | Holding Time | Grain Size(μm) | Elongation (%) | UTS (MPa) |
|---|---|---|---|---|---|---|
| 1 (Base 1) | - | - | - | 240 ± 38 | 11.5 ± 0.4 | 144.9 ± 1.5 |
| (Base 2) | - | - | - | 210 ± 32 | 23.2 ± 0.5 | 199.9 ± 2.9 |
| 2 (AlTiB) | - | - | - | 195 ± 27 | 26.0 ± 1.5 | 201.7 ± 3.3 |
| 3 | La | 0.2% | 20 min | 50 ± 5 | 31.0 ± 0.6 | 212.0 ± 2.1 |
| 4 | La | 0.4% | 15 min | 170 ± 21 | 29.2 ± 1.3 | 232.3 ± 2.7 |
| 5 | Er | 0.2% | 15 min | 130 ± 19 | 28.2 ± 1.9 | 207.9 ± 3.6 |
| 6 | Ce | 0.3% | 15 min | 80 ± 9 | 35.2 ± 0.9 | 206.2 ± 1.9 |
| 7 | Ce | 0.4% | 10 min | 78 ± 7 | 29.8 ± 2.0 | 244.9 ± 3.5 |
| 8 | Y | 0.2% | 10 min | 60 ± 6 | 29.7 ± 2.1 | 225.4 ± 3.7 |
| 9 | Y | 0.3% | 20 min | 65 ± 8 | 28.3 ± 1.7 | 223.3 ± 3.1 |
| 10 | Ce | 0.2% | 5 min | 75 ± 11 | 28.6 ± 0.7 | 252.6 ± 1.8 |
| 11 | Er | 0.4% | 20 min | 190 ± 23 | 25.9 ± 1.6 | 206.8 ± 2.8 |
| 12 | Y | 0.1% | 15 min | 65 ± 7 | 31.3 ± 2.2 | 212.4 ± 3.4 |
| 13 | La | 0.1% | 5 min | 60 ± 5 | 27.9 ± 0.3 | 211.6 ± 2.3 |
| 14 | Er | 0.3% | 5 min | 150 ± 20 | 27.6 ± 1.1 | 200.2 ± 2.6 |
| 15 | Ce | 0.1% | 20 min | 55 ± 4 | 32.0 ± 0.8 | 240.4 ± 2.2 |
| 16 | Er | 0.1% | 10 min | 65 ± 9 | 29.2 ± 0.3 | 215.0 ± 1.7 |
| 17 | Y | 0.4% | 5 min | 180 ± 24 | 27.8 ± 2.1 | 240.3 ± 3.9 |
| 18 | La | 0.3% | 10 min | 70 ± 10 | 26.2 ± 0.2 | 203.9 ± 1.6 |

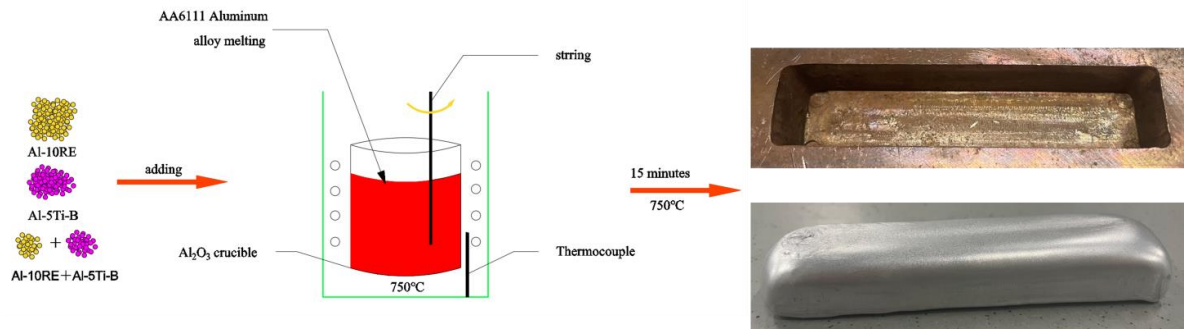



**Figure 1.** Experimental flow chart.

### *2.2. Specimen Characterizations*

The samples were examined for elemental content using an X-ray fluorescence spectrometer (XRF-S8 TIGER from BRUKER, Karlsruhe, Germany), and the elemental content of base 6111 is listed in Table 3. The microstructure was observed using an optical microscope with polarization. The samples were first polished by grinding in water with coarse to fine sandpaper, then polished and ultrasonically cleaned in alcohol before the grain size was observed by anodic cladding. The anodic coating etchant was a 1.8% mass fraction fluoroboric acid solution at a controlled voltage of 20 V for 80 s. The grain size was measured by the transversal method (GB/T 6394-2017) in Image-Pro Plus 6.0 imaging software (Media Cybernetics, Rockville, MD, USA). The samples of Al-5Ti-B and Al-5Ti-B + 0.1Ce master alloys (block of 15 mm × 15 mm × 5 mm) were polished with sandpaper, cleaned, and dried before being subjected to XRD (Rigaku D/MAX 2500V from Rigaku, Tokyo, Japan). The X-ray tube was a copper target with a scanning angle of 20–90°, a scanning speed of 5°/min, a tube voltage of 45 kV, and a tube current of 40 μA.

**Table 3.** Chemical compositions of the 6111 bases (wt.%).

| Element | Si | Mg | Cu | Fe | Mn | Zn | Ti | Cr | Al |
|---|---|---|---|---|---|---|---|---|---|
| Standard values | 0.6–1.1 | 0.5–1.1 | 0.5–0.9 | <0.4 | 0.1–0.45 | <0.15 | <0.1 | <0.1 | Bal. |
| Measured values | 1.09 | 0.57 | 0.59 | 0.21 | 0.18 | 0.04 | 0.02 | 0.01 | 97.29 |

The samples were first polished by sanding in water with coarse to fine sandpaper, then polished, ultrasonically cleaned in alcohol, and etched with Keller's reagent for 20 s. The tensile fracture specimens were ultrasonically cleaned and glued to the sample table with conductive adhesive. The specimens were ultrasonically cleaned and glued to the sample table with conductive adhesive. Three tensile samples were cut in the middle of each specimen and the results were averaged. According to GB/T228.1, the samples were processed into a national standard tensile sample, and the size of the tensile sample is shown in Figure 2. The specimens were subjected to the necessary tensile tests using a universal material testing machine (AGS-X 100KN) manufactured by Shimadzu, Kyoto, Japan, with a tensile speed of 1 mm/min, to investigate the effect of different rare earth master alloy refiners on the mechanical properties of the base alloy and determine the microstructure influence on mechanical properties.

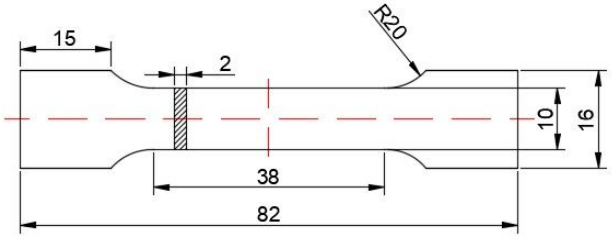



**Figure 2.** Tensile specimen shape and size (mm).

## 3. Results and Discussion

### *3.1. Microstructure of Al-5Ti-B-RE Refiner*

It is generally accepted that stable α-Al crystals result from heterogeneous nuclei and their growth. The theory suggests that the transfer of atoms from the melt to the α-Al phase is facilitated by substrates with high potency [24,25]. As shown in Figure 3, in this model [26], the nucleus α forms on the type-wall plane *W*, and α is a sphere crowned by the *W* plane. If the change in surface energy of the system during nucleation is $\Delta G_s$, then:

$$\Delta G_s = A_{\alpha L} \times \sigma_{\alpha L} + A_{\alpha W} \times \sigma_{\alpha W} - A_{\alpha W} \times \sigma_{LW}, \quad (1)$$

where $A_{\alpha L}$ and $A_{\alpha W}$ are the interface areas between nucleus α and liquid phase *L* and type wall *W*, respectively;$\sigma_{\alpha L}$, $\sigma_{\alpha W}$, $\sigma_{LW}$ are the specific surface energy (expressed as surface tension) at the α-*L*, α-*W*, *L*-*W* interfaces, respectively. At the intersection of the three phases, the surface tension should reach equilibrium, and the collation can be obtained as follows:

$$\Delta G_s = (A_{\alpha L} - \pi r^2 \sin^2\theta \cos\theta)\sigma_{\alpha L}, \quad (2)$$

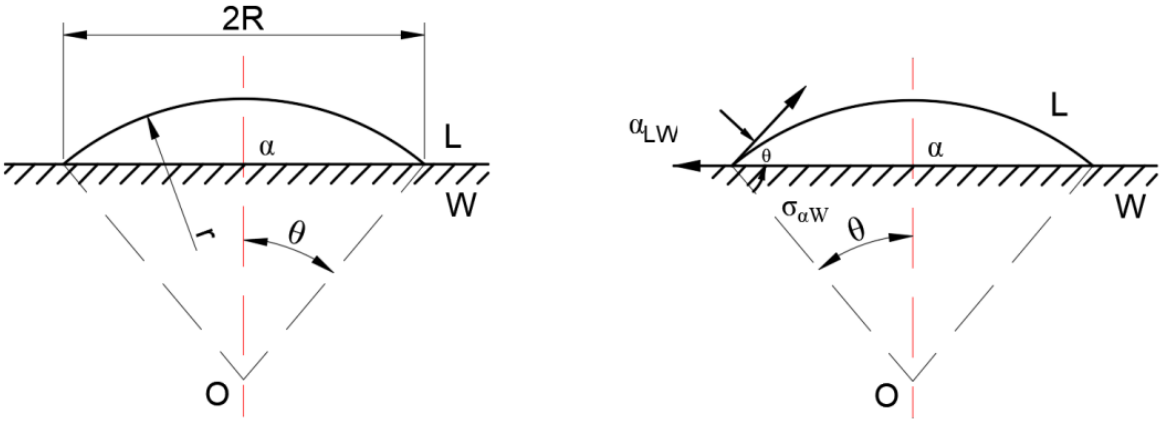



**Figure 3.** Schematic diagram of heterogeneous nucleation.

The total free energy change of the system when the nucleus is nucleated:

$$\Delta G = \Delta G_t + \Delta G_s = (\frac{4}{3}\pi r^3 \Delta G_v + 4\pi r^2 \sigma_{\alpha L}) f(\theta), \quad (3)$$

where $\Delta G_t$ is the change in nucleation caused by volume:

$$f(\theta) = (2 - 3\cos\theta + \cos^3\theta)/4, \quad (4)$$

Since $\theta$ is in the range of 0–180°, $f(\theta)$ must be less than 1. The work required for heterogeneous nucleation is less than that for uniform nucleation, so the subcooling is smaller and easier to nucleate. The nucleation rate increases as the work needed to form stable crystals decreases. Therefore, the more nucleation sites and the better the lattice match, the better the grain refinement [27].

Effective grain refinement by the Al-5Ti-1B grain refiner was directly attributed to the enhanced potency of $TiB_2$ particles with the $Al_3Ti$ [28]. In Figure 4, the morphology and distribution of the nucleated phases of the master alloy can be clearly seen after corrosion with Keller's reagent, and the Al-5Ti-B refiner showed obvious large particles and clusters. The addition of rare earth not only reduced the particle size, it also made the particles more dispersed. When combining the energy spectra in Figure 5 and the XRD patterns in Figure 6, it can be seen that the $Al_3Ti$ phase of Al-5Ti-B had long strips, and the long strips of $Al_3Ti$ and clusters limited its refinement effect. The $Al_3Ti$ phase of Al-5Ti-B was finer and

more uniformly dispersed with the addition of rare earth, and the clustering phenomenon was improved.

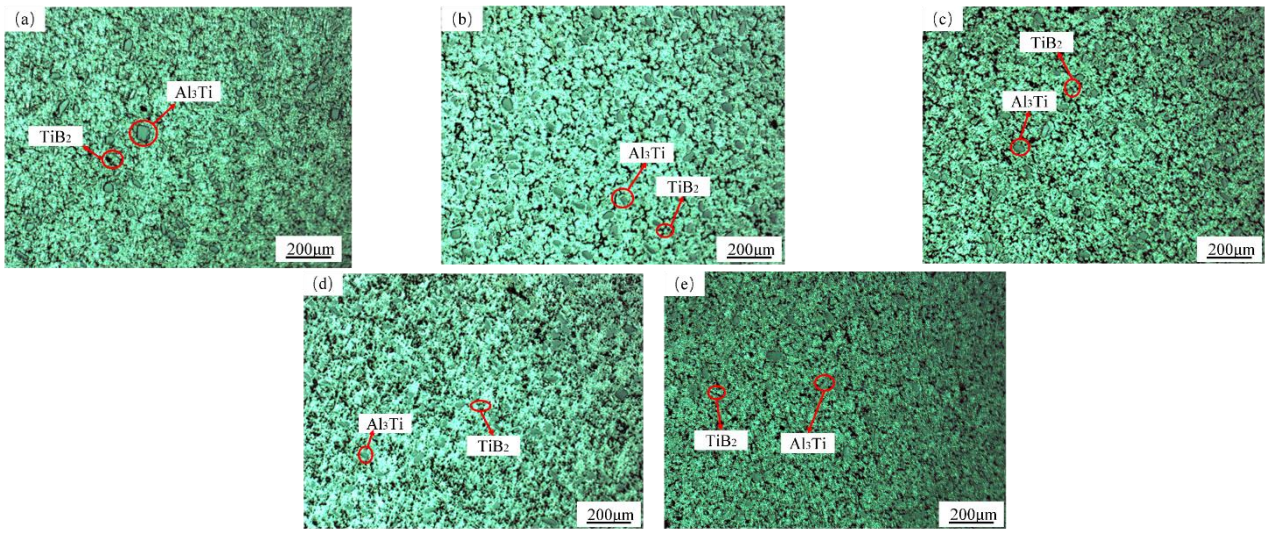



**Figure 4.** Optical micrographs of the refiners (**a**) Al-5Ti-B refiner; (**b**) Al-5Ti-B + La refiner; (**c**) Al-5Ti-B + Er refiner; (**d**) Al-5Ti-B + Y refiner; (**e**) Al- 5Ti-B + Ce refiner.

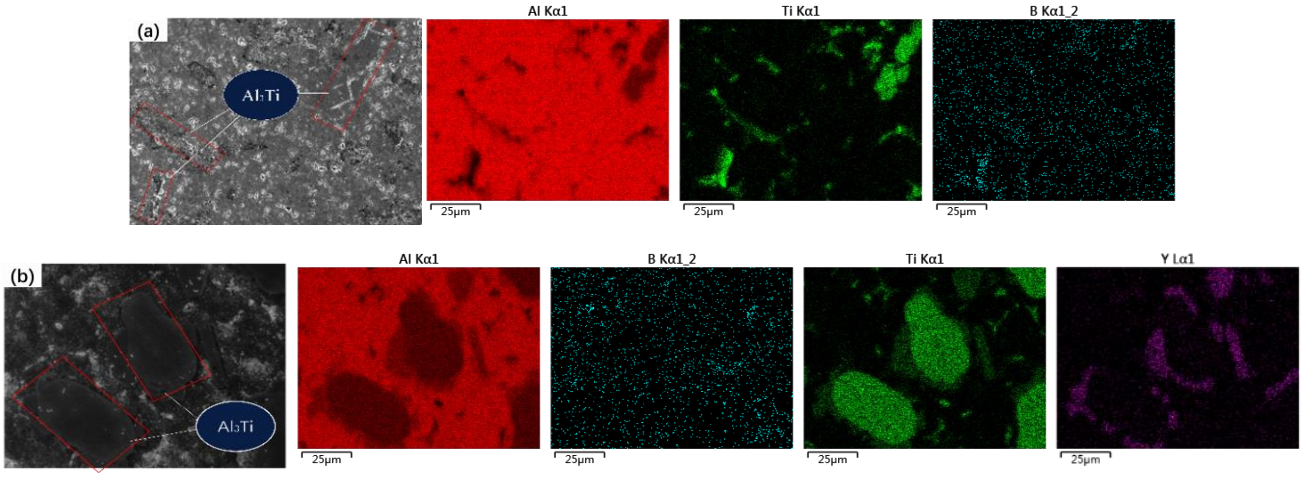



**Figure 5.** SEM/EDS micrographs of the master alloys (**a**) Al-5Ti-B; (**b**) Al-5Ti-B-0.2Y.

Figure 6 shows the XRD results for the Al-5Ti-B and Al-5Ti-B + 0.1Ce refiners. The results showed that the α-Al, $Al_3Ti$, and $TiB_2$ phases were present in both refiners, while the $Ti_2Al_{20}Ce$ phase was also present in the Al-5Ti-B-RE refiner. The corresponding rare earth phases were present in all four refiners with rare earth additions. So, more particles could become effective nucleation substrates.

The addition of rare earth Ce to the master alloy added a rare earth phase to the melt. The decomposition of the rare earth phase released Ce, which spontaneously deviated on the $TiAl_3$ surface. On the one hand, it inhibited the growth of $TiAl_3$, thus allowing more particles to become effective nucleation substrates. On the other hand, it reduced the surface energy of $TiAl_3$ and promoted the nucleation of α-Al on the $TiAl_3$ surface.

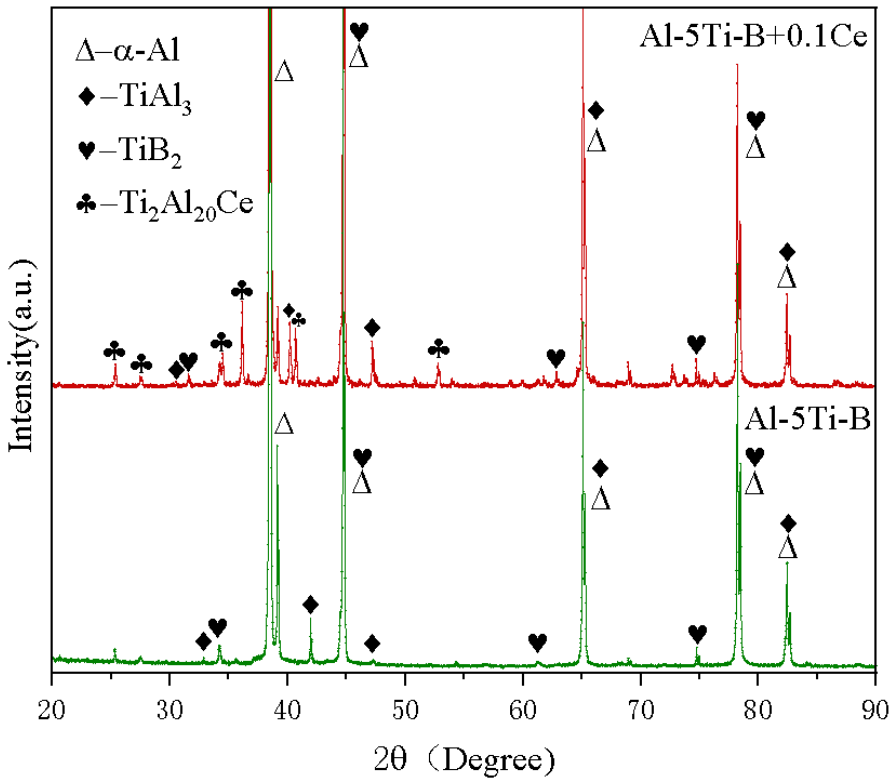



**Figure 6.** XRD patterns of Al-5Ti-B and Al-5Ti-B + 0.1Ce.

### *3.2. Evaluation of the Refinement Effect of Different Master Alloys on 6111 Aluminum Alloy*

In order to better control the efficiency of grain refinement, Easton [29] and John [30] developed a new analytical model for grain refinement in which the grain size, $d$ [31,32], can be expressed as:

$$d = \frac{1}{\sqrt[3]{f \cdot \rho v}} + \frac{D \cdot \Delta T_n}{v \cdot Q}, \quad (5)$$

where $\rho_v$ refers to the volume number density of nucleated particles; $f$ refers to the fraction of activated particles; $D$ is the diffusion coefficient; and $v$ is the growth rate. $\Delta T_n$ is the subcooling required for nucleation; $Q$ is the growth limiting factor, $Q = m \cdot k^{-1} C_0$, $m$ is the slope of the liquid phase line, and $k$ is the distribution system number, $C_0$ is the concentration of solute [33]. Equation (5) can be simplified to $d = a + \frac{b}{Q}$ where $\alpha$ is related to the number of activated nuclei. The potency of the nucleate particles is related to $b$ and the solute segregation is related to $Q$ [34].

The Al-Ti-B refiner has been used extensively since its introduction. It produces two important refining phases in the melt ($Al_3Ti$, $TiB_2$), which play a key role in refining the grain of aluminum alloys. The addition of rare earth elements results in the homogeneous dispersion of these two important refining phases in the melt, leading to an increased number of activation nuclei. At the same time, the rare earth elements segregate at the grain boundaries, producing a greater growth restriction factor [35]. However, the addition of rare earth elements is not always effective. Too many or too long holding times can lead to coarsening of the grains [36]. In this research, the addition of 0.3% Ce under a longer holding time of 15 min led to the degradation of performance. The microstructure of specimens refined with different refiners is illustrated in Figure 7. The results showed that the 6111 poured into the steel mold had a significant coarse grain and obvious dendrites. But the 6111 poured into the copper mold tended to form equiaxed grains due to the large supercooling, and the grain refinement effect was more limited. With the right amount of addition and the right holding time, all four different additions of rare earth produced a

significant grain refinement effect, forming fine isometric crystals, which played a key role in the performance improvement.

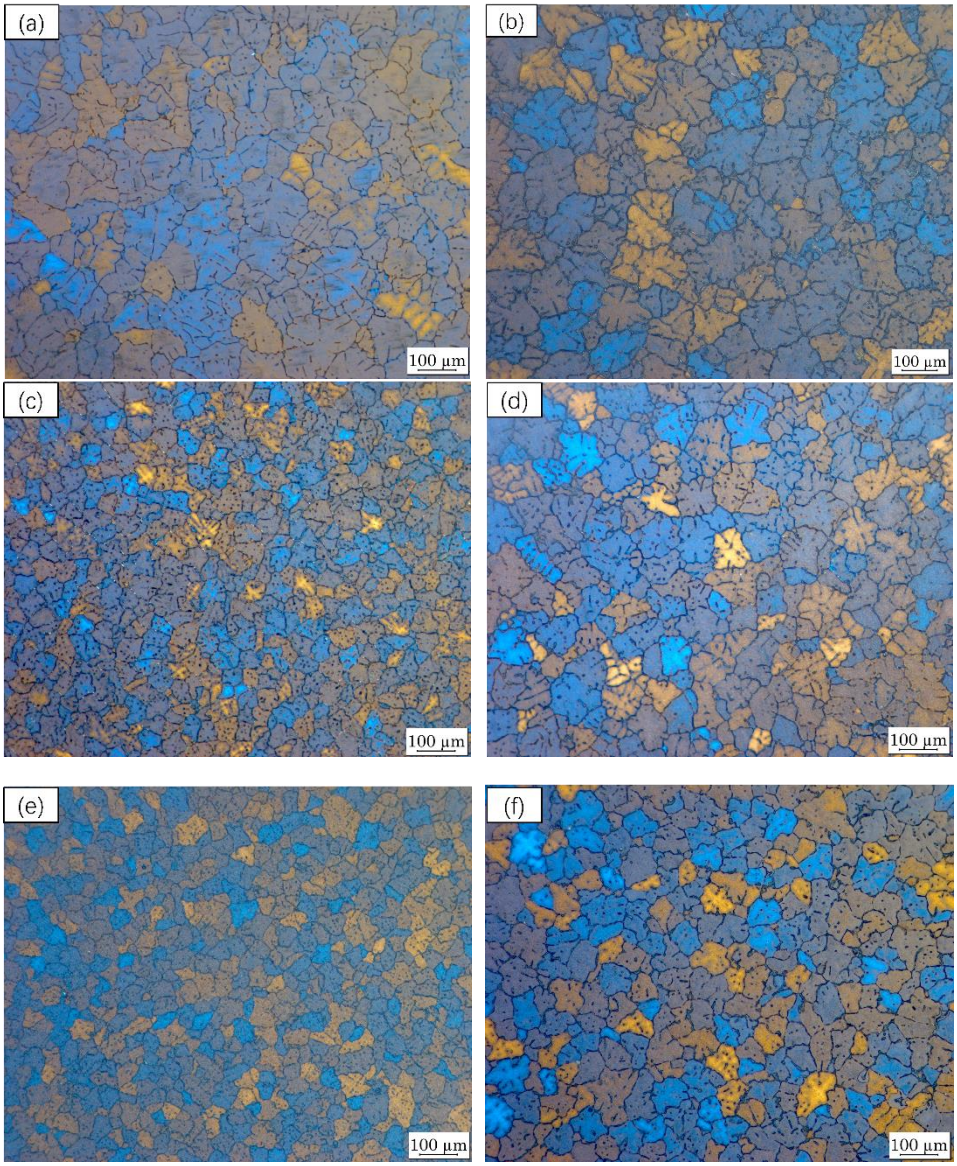



**Figure 7.** Microstructure of specimens refined with different refiners: (**a**) 6111 (copper mold); (**b**) Al-5Ti-B/6111; (**c**) Al-5Ti-B + 0.2% La/6111; (**d**) Al-5Ti-B + 0.2% Er/6111; (**e**) Al-5Ti-B + 0.2% Y/6111; (**f**) Al-5Ti-B + 0.2% Ce/6111.

In order to study the primary and secondary effects of different factors on grain size, range analysis was used to analyze the impact of the results, and the statistical results obtained are shown in Table 4. From Table 4, the extreme difference values of the three factors on the grain size in descending order were earth content > rare earth type > holding time. It can be seen that the addition of rare earth to the Al-5Ti-B refiner does not need to be a lot to achieve good grain refinement, and it is worth noting that the rare earth Ce was the best in terms of grain refinement. Whether the holding time was 5 min or 20 min, the refinement effect of Al-5Ti-B + Ce was relatively stable, showing good resistance to recession and greatly improving the microstructure of the cast 6111 aluminum alloy.

**Table 4.** Analysis of grain size in orthogonal experiment.

| Parameter | Rare Earth Types | Rare Earth Content | Holding Time |
|---|---|---|---|
| K1 | 87.50 μm | 61.25 μm | 116.25 μm |
| K2 | 133.75 μm | 78.75 μm | 68.25 μm |
| K3 | 92.50 μm | 91.25 μm | 111.25 μm |
| K4 | 72.00 μm | 154.50 μm | 90.00 μm |
| Extreme difference values | 61.75 μm | 93.25 μm | 48.00 μm |
| Optimum solution | Ce | 0.1% | 10 min |

Order of importance Rare earth content > Rare earth type > Holding time.

Based on the grain size analysis by orthogonal experiment, the optimum rare earth and optimum rare earth content were taken and single-factor experiments were carried out on the holding time in order to investigate the anti-recession effect of Al-5Ti-B-0.1Ce refined 6111.The Al-5Ti-B-0.1Ce/6111 specimens with different holding times were polished and then etched with a mixture of acids (45 mL HCl, 15 mL $HNO_3$, 15 mL HF, 25 mL $H_2O$) to observe the macrostructure in order to compare the refinement effect. The results are shown in Figure 8. The results showed that the grain size of the Al-5Ti-B-0.1Ce/6111 specimens did not become significantly coarser from a holding time of 5 min to a holding time of 20 min, indicating that the Al-5Ti-B-0.1Ce refinement of the 6111 aluminum had a good effect on anti-recession.

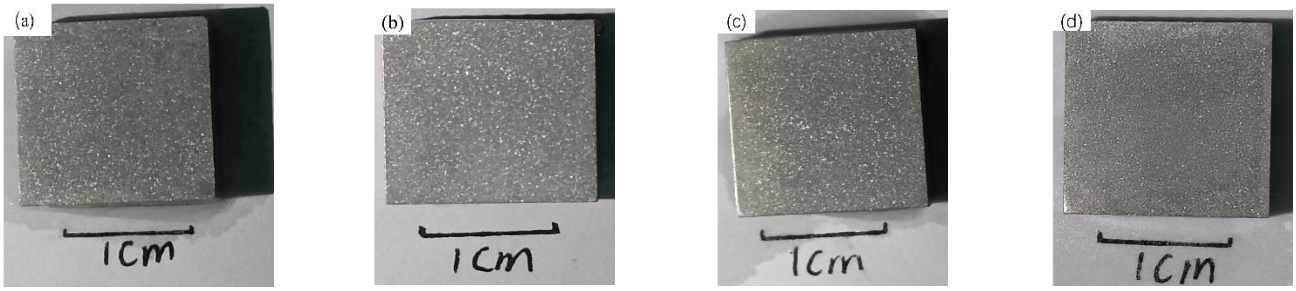



**Figure 8.** Macrostructure of Al-5Ti-B-0.1Ce/6111: (**a**) Holding for 5 min; (**b**) Holding for10 min; (**c**) Holding for 15 min; (**d**) Holding for 20 min.

### *3.3. Impact of the Second Phase*

In order to investigate the synergistic effect of Al-5Ti-B and rare earth on the as-cast structure and properties of 6111 aluminum alloy, the effect of the addition of Al-5Ti-B and rare earth on their physical phases was first investigated by thermodynamic calculation. The equilibrium phase diagrams of the Al-5Ti-B/6111 and Al-5Ti-B-0.1Ce/6111 systems are shown in Figure 9. The Al-5Ti-B/6111 system consisted mainly of α-Al, $Al_5Cu_2Mg_8Si_6$, $Mg_2Si$, α-Fe(AlFeMnSi), β-Fe(AlFeSi) phases, a small number of classical nucleation phases $Al_3Ti$, $TiB_2$, and trace amounts of $Al_{13}Cr_4Si_4$. In the early stages of compound formation, first came the formation of the stable high-temperature $TiB_2$ phase, which played a key role in heterogeneous nucleation, while the basis for refining the grain was laid with the cooperation of $Al_3Ti$. The α-$Al_{15}(Mn,Fe)_3Si_2$ phase and β-$Al_5FeSi$ phase formation was also critical, as the form of the Fe element present tends to have a great influence on the matrix, with the α-$Al_{15}(Mn,Fe)_3Si_2$ phase having less influence on the mechanical properties of the matrix, while the β-$Al_5FeSi$ phase, in a plate-like form, severely cuts into the matrix and significantly reduces the mechanical properties of the aluminum alloys. As the temperature decreased, the $Mg_2Si$ phase was gradually formed, which was considered to be a good reinforcing phase and gave the matrix better mechanical properties. The Ce-rich phase decomposed the Ce elements at high temperatures, and the Ce elements at the grain boundaries restricted the growth of α-Al, resulting in the formation of fine grains.

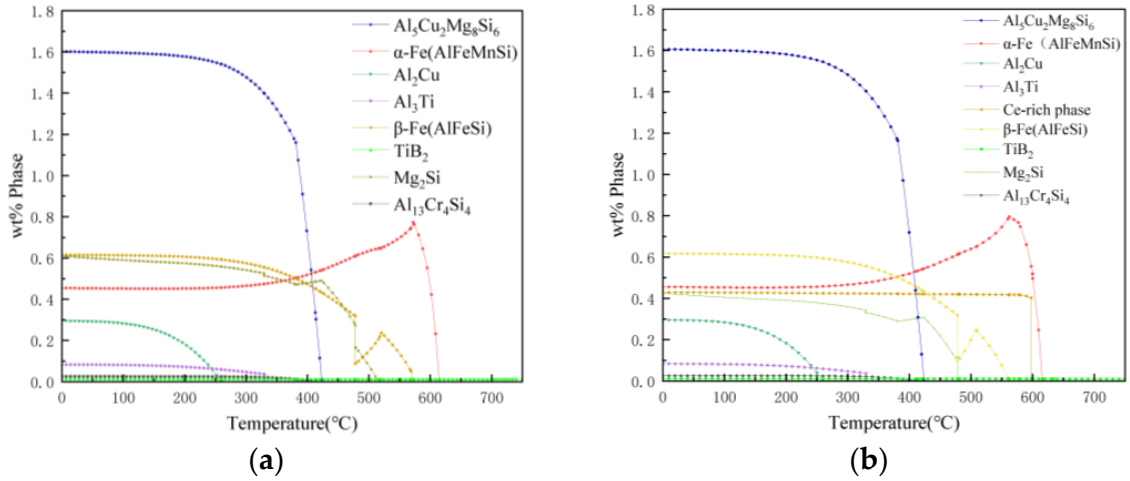



**Figure 9.** Phase fraction as a function of temperature at equilibrium for: (**a**) Al-5Ti-B/6111; (**b**) Al-5Ti-B-0.1Ce/6111.

To further investigate the effect of Al-5Ti-B and Ce on the phase composition of 6111, thermodynamic simulations were performed for the Al-5Ti-B/6111 and Al-5Ti-B + 0.1Ce/6111 systems [37]. Figure 10 shows the solid phase fraction versus temperature in the Scheil solidification path and the effect of the addition of rare earth on the nucleation temperature. The Scheil solidification model is based on the assumption that the solute does not diffuse in the solid phase and is perfectly homogeneous in the liquid phase [38]. It has been widely used to model the as-cast microstructure of non-equilibrium solidifying alloys. Firstly, for the nucleation temperature of α-Al, there was a small increase in the nucleation temperature of α-Al with the addition of the rare earth element Ce, which further confirmed that the decomposition of the Ce-rich phase released the element Ce, which biased the $Al_3Ti$ before it solidified and inhibited the growth of $Al_3Ti$. As a result, this led to more particles becoming effective nucleation substrates, reducing the subcooling required for α-Al nucleation and making it easier to nucleate. In addition, the nucleation temperature of the α-$Al_{15}(Mn,Fe)_3Si_2$ phase increased while that of the β-$Al_5FeSi$ phase decreased. This was because the addition of Ce promoted the nucleation of the α-$Al_{15}(Mn,Fe)_3Si_2$ phase and inhibited the nucleation of the β-$Al_5FeSi$ phase, which promoted the transformation of the β-$Al_5FeSi$ phase to the α-$Al_{15}(Mn,Fe)_3Si_2$ phase and reduced the harm to the mechanical properties of the matrix.

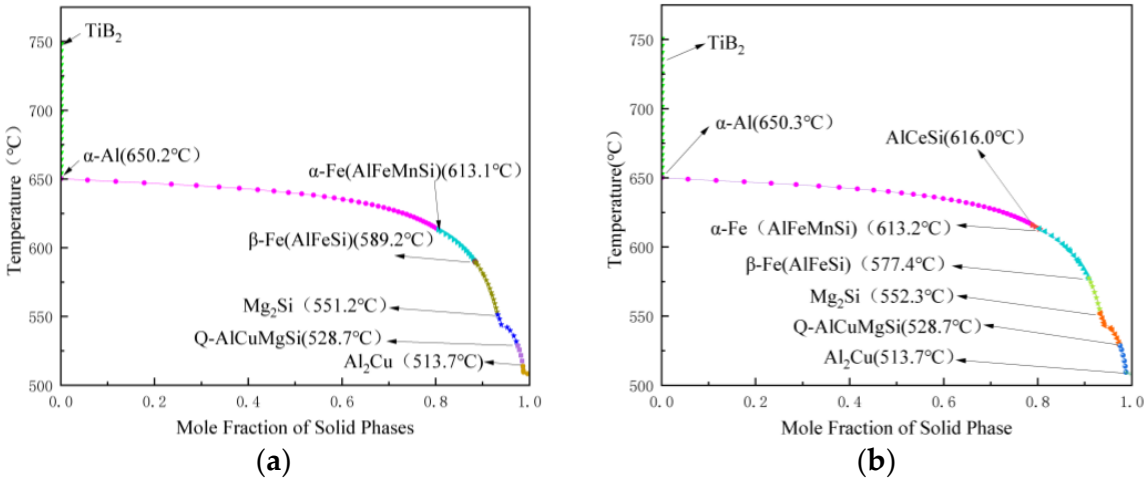



**Figure 10.** Solidification path of the alloy: (**a**) Al-5Ti-B/6111; (**b**) Al-5Ti-B + 0.1Ce/6111.

### *3.4. Analysis of the Mechanical Properties of the Cast State*

In terms of tensile properties, the base strength was 144.9 MPa and the plasticity was 11.5% when poured into the steel mold. Still, its strength was 199.9 MPa and the plasticity was 23.2% when poured into the copper mold, indicating that the cooling rate had a profound effect on the properties of the alloy. Therefore, subsequent tests were carried out using copper molds as casting molds. The addition of Al-5Ti-B resulted in an almost constant strength and a slight increase in elongation, indicating that grain refinement contributed significantly to the elongation, which reduced the density of dislocations dispersed within each grain, thus allowing the material to resist greater plastic deformation.

Figure 11 shows the stress–strain curves for the cast alloys. It can be seen from the graph, that the mechanical properties of the alloys were improved by the addition of rare earth, with the best elongation being 35.2% for Al-5Ti-B-0.3Ce/6111, and the highest tensile strength being 252.6 MPa for Al-5Ti-B-0.2Ce/6111.The best comprehensive mechanical property was achieved by Al-5Ti-B-0.1Ce/6111, with a tensile strength of 240.4 MPa and an elongation of 32.0%.

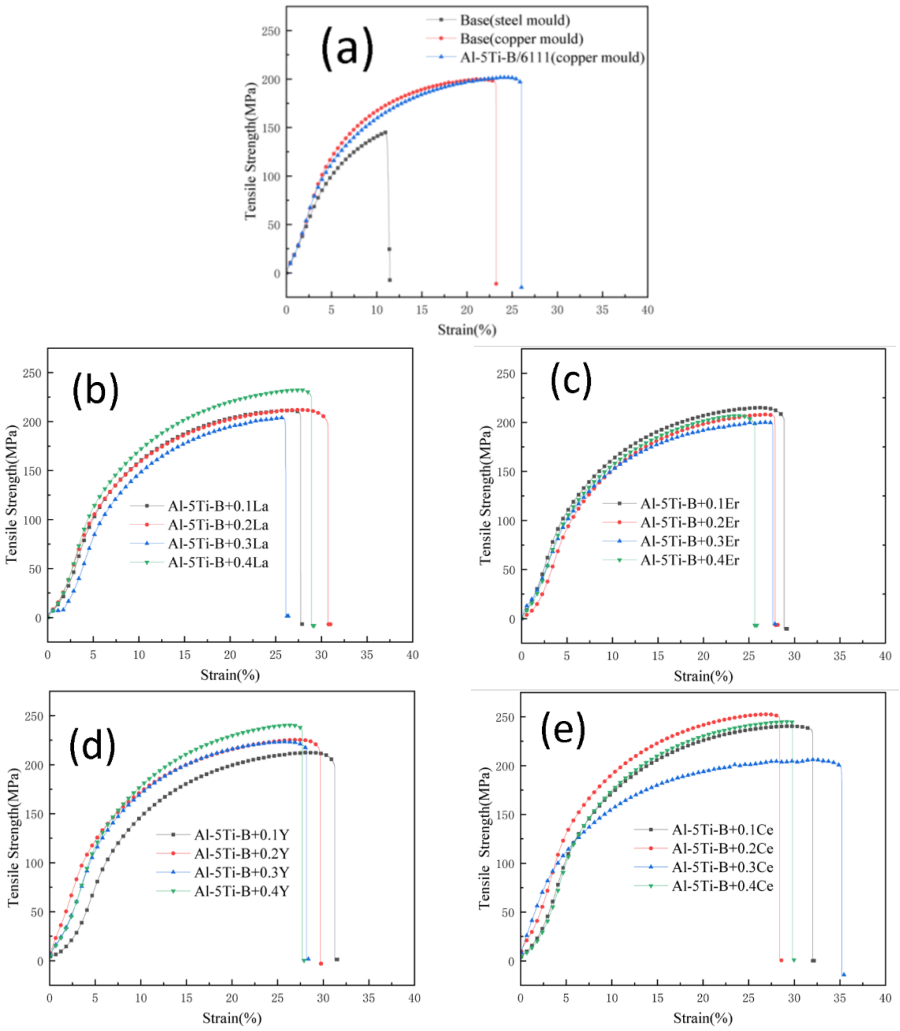



**Figure 11.** Stress–strain curves for cast alloys: (**a**) base; (**b**) Al-5Ti-B + La/6111; (**c**) Al-5Ti-B + Er/6111; (**d**) Al-5Ti-B + Y/6111; (**e**) Al-5Ti-B + Ce/6111.

In order to study the major and minor influences of different factors on mechanical properties, range analysis was used to analyze the influence of the results, and the statistical results obtained are shown in Tables 5 and 6. The order of the extreme differences in the effects of the three factors on elongation from largest to smallest was rare earth type > holding time > rare earth content. At the same time, the extreme difference between

the three factors on the tensile strength was also the largest for the rare earth type, indicating that the rare earth type had a greater influence on the mechanical properties, which may have been related to the rare earth phase formed and its solid solution degree. It is worth noting that the best solution for elongation was 0.1%, while the best solution for tensile strength was 0.4%. The main reason for this was that fewer rare earth tended to disperse and lead to finer grains, while too much agglomeration led to coarser grains, but more rare earth increased tensile strength.

**Table 5.** Analysis of elongation in orthogonal experiment.

| Parameter | Rare Earth Types | Rare Earth Content | Holding Time |
|---|---|---|---|
| K1 | 28.57% | 30.09% | 27.97% |
| K2 | 27.71% | 29.36% | 28.73% |
| K3 | 29.26% | 29.35% | 30.96% |
| K4 | 31.41% | 28.15% | 29.30% |
| Extreme difference values | 3.7% | 1.94% | 2.99% |
| Optimum solution | Ce | 0.1% | 15 min |

Order of influence: Rare Earth Types > Holding Time > Rare Earth Content.

**Table 6.** Analysis of ultimate tensile strength in orthogonal experiment.

| Parameter | Rare Earth Types | Rare Earth Content | Holding Time |
|---|---|---|---|
| K1 | 214.96 MPa | 219.86 MPa | 226.18 MPa |
| K2 | 207.49 MPa | 224.48 MPa | 222.31 MPa |
| K3 | 225.38 MPa | 208.41 MPa | 214.71 MPa |
| K4 | 236.02 MPa | 231.10 MPa | 220.65 MPa |
| Extreme difference values | 28.53 MPa | 22.69 MPa | 11.47 MPa |
| Optimum solution | Ce | 0.4% | 5 min |

Influence: Primary Rare Earth Type > Rare Earth Content > Holding Time.

### *3.5. Cast Fracture Analysis*

Figure 12 shows the fracture morphology of the six alloys. The 6111 base had obvious holes and ridge-like fractures, with hard-to-observe tough nests, but obvious tearing ridges. With the addition of Al-5Ti-B, the porosity and fracture surface was reduced, while small amounts of tough nests and deconstruction surfaces were present, which is a mixed fracture. After the addition of rare earth, a large number of tough nests appear in the fractures, especially in the Al-5Ti-B-0.1Ce/6111 alloy, where large and deep tough nests were evident in the fractures and no facets were observed, but the Al-5Ti-B-0.1Er/6111 alloy still had more cleavage plane in the fractures, which corresponded to their mechanical properties.

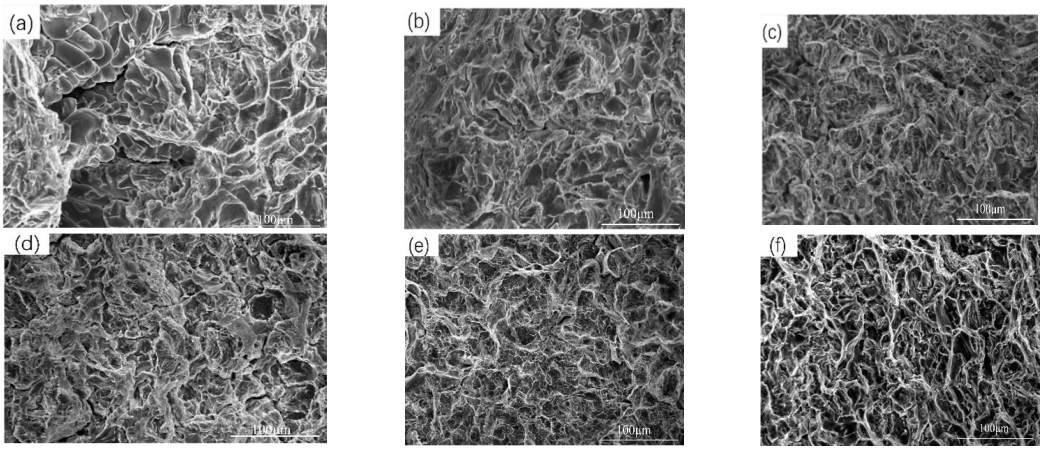



**Figure 12.** Fracture features: (**a**) 6111; (**b**) Al-5Ti-B/6111; (**c**) Al-5Ti-B-0.1La/6111; (**d**) Al-5Ti-B-0.1Er/6111; (**e**) Al-5Ti-B-0.1Y/6111; (**f**) Al-5Ti-B-0.1Ce/6111.

## 4. Conclusions

(1) Among the four rare earths, Al-5Ti-B + Ce had the best effect on the grain refinement and mechanical properties of the 6111 aluminum, and had the best fracture morphology.

(2) The addition of rare earth to the Al-5Ti-B added a rare earth-rich phase to the $TiAl_3$ phase and the $TiB_2$ phase, and the decomposition of the rare earth phase released rare earth elements, which made $TiB_2$ difficult to aggregate or deposit and inhibited the growth of $TiAl_3$, thus resulting in more particles becoming an effective nucleation substrate.

(3) The influence of the $\alpha$-$Al_{15}(Mn,Fe)_3Si_2$ phase on the mechanical properties of the base was small. In contrast, the plate-like $\beta$-$Al_5FeSi$ phase severely cut into the base and significantly reduced the mechanical properties of the aluminum alloy. Compared to the base 6111, the addition of rare earth facilitated the transformation of the $\beta$-$Al_5FeSi$ phase into the $\alpha$-$Al_{15}(Mn,Fe)_3Si_2$ phase.

(4) In the as-cast state, Al-5Ti-B + 0.1Ce/6111 had the best comprehensive mechanical properties. It was found that the addition of Al-5Ti-B + 0.1Ce, which had an ultimate tensile strength of 240.4 $\pm$ 2.2 MPa, successfully reduced the grain size by 73.8% and improved elongation by 37.8% compared to the base alloy.

**Author Contributions:** Conceptualization, C.M. and H.T.; methodology, Z.L. and C.M.; validation, C.M., C.S. and Y.L.; investigation, C.S. and D.L.; resources, C.M.; data curation, H.T.; writing—original draft preparation, C.M. and Z.L.; writing—review and editing, C.M. and D.L.; visualization, C.S.; supervision, X.R. and J.W.; project administration, H.T.; funding acquisition, H.T. and J.W. All authors have read and agreed to the published version of the manuscript.

**Funding:** This research was funded by the National Natural Science Foundation of China-Guangxi Joint Fund (U20A20276), and the Innovation and Entrepreneurship Training Program for College Students in Guangxi (202210593049).

**Data Availability Statement:** Not applicable.

**Conflicts of Interest:** The authors declare no conflict of interest.

## References

1. Wang, K.; Jiang, H.Y.; Jia, Y.W.; Zhou, H.; Wang, Q.D.; Ye, B.; Ding, W.J. Nanoparticle-inhibited growth of primary aluminum in Al-10Si alloys. *Acta Mater.* **2016**, *103*, 252–263. [CrossRef]
2. Deepati, A.K.; Alhazmi, W.; Benjeer, I. Mechanical characterization of AA5083 aluminum alloy welded using resistance spot welding for the lightweight automobile body fabrication. *Mater. Today Proc.* **2021**, *45*, 5139–5514. [CrossRef]
3. Bolzoni, L.; Nowak, M.; Babu, N.H. Grain refinement of Al-Si alloys by Nb-B inoculation. Part II: Application to commercial alloys. *Mater. Design* **2015**, *66*, 376–383. [CrossRef]
4. Abdizadeh, H.; Ashuri, M.; Moghadam, P.T.; Nouribahadory, A.; Baharvandi, H.R. Improvement in physical and mechanical properties of aluminum/zircon composites fabricated by powder metallurgy method. *Mater. Design* **2011**, *32*, 4417–4423. [CrossRef]
5. Murty, B.S.; Kori, S.A.; Chakraborty, M. Grain refinement of aluminum and its alloys by heterogeneous nucleation and alloying. *Int. Mater. Rev.* **2002**, *47*, 3–29. [CrossRef]
6. Birol, Y. A novel Al-Ti-B alloy for grain refining Al-Si foundry alloys. *J. Alloys Compd.* **2009**, *486*, 219–222. [CrossRef]
7. Birol, Y. Performance of AlTi5B1, AlTi3B3 and AlB3 master alloys in refining grain structure of aluminum foundry alloys. *Mater. Sci. Technol.* **2012**, *28*, 481–486. [CrossRef]
8. Wang, Z.J.; Si, N.C. Synthesis and Refinement Performance of the Novel Al-Ti-B-RE Master Alloy Grain Refiner. *Rare Met. Mater. Eng.* **2015**, *44*, 2970–2975.
9. Li, Y.; Hu, B.; Liu, B.; Nie, A.; Gu, Q.; Wang, J.; Li, Q. Insight into Si poisoning on grain refinement of Al-Si/Al-5Ti-B system. *Acta Mater.* **2020**, *187*, 51–65. [CrossRef]
10. Mao, G.; Tong, G.; Gao, W.; Liu, S.; Zhong, L. The poisoning effect of Sc or Zr in grain refinement of Al-Si-Mg alloy with Al-Ti-B. *Mater. Lett.* **2021**, *302*, 130428. [CrossRef]
11. Wang, J.; Horsfield, A.; Schwingenschlögl, U.; Lee, P.D. Heterogeneous nucleation of solid Al from the melt by TiB 2 and Al 3 Ti: An ab initio molecular dynamics study. *Phys. Rev. B* **2010**, *82*, 184203. [CrossRef]
12. Wu, J.; Ruan, Q.; Chen, S.; Meng, C.; Xu, Z.; Wei, C.; Wang, J. Insights into Poisoning Mechanism of Zr by First Principle Calculation on Adhesion Work and Adsorption Energy between TiB2, Al3Ti, and Al3Zr. *Metals* **2022**, *12*, 286. [CrossRef]

13. Nie, J.; Ma, X.; Ding, H.; Liu, X. Microstructure and grain refining performance of a new Al-Ti-C-B master alloy. *J. Alloys Compd.* **2009**, *486*, 185–190. [CrossRef]
14. Xu, J.; Li, Y.; Ma, K.; Fu, Y.; Guo, E.; Chen, Z.; Li, Q. In-situ observation of grain refinement dynamics of hypoeutectic Al-Si alloy inoculated by Al-Ti-Nb-B alloy. *Scr. Mater.* **2020**, *187*, 142–147. [CrossRef]
15. Zhang, Y.H.; Ye, C.Y.; Shen, Y.P.; Chang, W.; StJohn, D.H.; Wang, G.; Zhai, Q.J. Grain refinement of hypoeutectic Al-7wt.% Si alloy induced by an Al-V-B master alloy. *J. Alloys Compd.* **2020**, *812*, 152022. [CrossRef]
16. Vicario, I.; Poulon, Q.A.; Lagos, M.A.; Silvain, J.F. Effect of material and process atmosphere in the preparation of Al-Ti-B grain refiner by SHS. *Metals* **2015**, *5*, 1387–1396. [CrossRef]
17. Mohanty, P.S.; Guthrie, R.I.L.; Gruzleski, J.E. Studies on the fading behaviour of Al-Ti-B master alloys and grain refinement mechanism using LiMCA. Light Metals: Proceedings of Sessions, TMS Annual Meeting, Warrendale, PA, USA. 1995; pp. 859–868.
18. Qian, P.P.; Tang, Z.H.; Yuan, M.W.; Xiang, Y.L.; Wang, L. Microstructure and refinement mechanism of TiB2/TiAl3 in remelted Al-5Ti-1B system. *Mater. Sci. Technol.* **2019**, *35*, 1563–1571. [CrossRef]
19. Zhao, Y.L.; He, W.X.; Song, D.F.; Shen, F.H.; Li, X.X.; Sun, Z.Z.; Wang, Y.; Liu, S.H.; Du, Y.; Fernández, R. Effect of ultrasonic melt processing and Al-Ti-B on the microstructural refinement of recycled Al alloys. *Ultrason. Sonochem.* **2022**, *89*, 106139. [CrossRef]
20. Liu, X.; Wang, B.; Li, Q.; Wang, J.; Zhang, C.; Xue, C.; Tang, H. Quantifying the Effects of Grain Refiners Al-Ti-B and La on the Microstructure and Mechanical Properties of W319 Alloy. *Metals* **2022**, *12*, 627. [CrossRef]
21. Ding, W.; Zhao, X.; Chen, T.; Zhang, H.; Liu, X.; Cheng, Y.; Lei, D. Effect of rare earth Y and Al-Ti-B master alloy on the microstructure and mechanical properties of 6063 aluminum alloy. *J. Alloys Compd.* **2020**, *830*, 154685. [CrossRef]
22. Ma, T.F.; Chen, Z.Y.; Nie, Z.R.; Huang, H. Microstructure of Al-Ti-B-Er refiner and its grain refining performance. *J. Rare Earths* **2013**, *31*, 622–627. [CrossRef]
23. Chen, Z.Q.; Hu, W.X.; Shi, L.; Wang, W. Effect of rare earth on morphology and dispersion of TiB2 phase in Al-Ti-B alloy refiner. *China Foundry* **2023**, 1–10. [CrossRef]
24. Du, Q.; Li, Y.J. An extension of the Kampmann–Wagner numerical model towards as-cast grain size prediction of multicomponent aluminum alloys. *Acta Mater.* **2014**, *71*, 1359–6454. [CrossRef]
25. Bolzoni, L.; Babu, N.H. Engineering the heterogeneous nuclei in Al-Si alloys for solidification control. *Appl. Mater. Today* **2016**, *5*, 255–259. [CrossRef]
26. Gottstein, G. *Physical Foundations of Materials Science*; Springer: Berlin/Heidelberg, Germany, 2013.
27. Ma, S.; Zong, N.; Dong, H.; Jing, T. Effect of Al-V-B grain refiner on refining aluminium alloys: Estimation from ab initio calculations. *Mater. Sci. Eng.* **2020**, *861*, 012047. [CrossRef]
28. Fan, Z.; Wang, Y.; Zhang, Y.; Fan, Z.; Wang, Y.; Zhang, Y.; Qin, T.; Zhou, X.R.; Thompson, G.E.; Pennycook, T.; et al. Grain refining mechanism in the Al/Al-Ti-B system. *Acta Mater.* **2015**, *84*, 292–304. [CrossRef]
29. Easton, M.; StJohn, D. An analysis of the relationship between grain size, solute content, and the potency and number density of nucleant particles. *Metall. Mater. Trans. A* **2005**, *36*, 1911–1920. [CrossRef]
30. Easton, M.A.; StJohn, D.H. A model of grain refinement incorporating alloy constitution and potency of heterogeneous nucleant particles. *Acta Mater.* **2001**, *49*, 1867–1878. [CrossRef]
31. StJohn, D.H.; Qian, M.; Easton, M.A.; Cao, P. The Interdependence Theory: The relationship between grain formation and nucleant selection. *Acta Mater.* **2011**, *59*, 4907–4921. [CrossRef]
32. Qian, M.; Cao, P.; Easton, M.A.; McDonald, S.D.; StJohn, D.H. An analytical model for constitutional supercooling-driven grain formation and grain size prediction. *Acta Mater.* **2010**, *58*, 3262–3270. [CrossRef]
33. Quested, T.E.; Dinsdale, A.T.; Greer, A.L. Thermodynamic modelling of growth-restriction effects in aluminium alloys. *Acta Mater.* **2005**, *53*, 1323–1334. [CrossRef]
34. StJohn, D.H.; Cao, P.; Qian, M.; Easton, M.A. A new analytical approach to reveal the mechanisms of grain refinement. *Adv. Eng. Mater.* **2007**, *9*, 739–746. [CrossRef]
35. Wang, X.; Cong, X.; Muhammad, A.; Hanada, S.; Yamagata, H.; Wang, W.H. Effects of Al-Ti-B-RE grain refiner on microstructure and mechanical properties of Al-7.0 Si-0.55 Mg alloy. *Trans. Nonferr. Met. Soc. China* **2014**, *24*, 2244–2250. [CrossRef]
36. Liu, X.; Wang, B.; Li, Q.; Wang, J.; Xue, C.; Yang, X.; Liu, X. Quantifying the effects of grain refiners (AlTiB and Y) on microstructure and properties in W319 alloys. *Mater. Today Commun.* **2022**, *33*, 104671. [CrossRef]
37. Zhan, H.; Hu, B. Analyzing the microstructural evolution and hardening response of an Al-Si-Mg casting alloy with Cr addition. *Mater. Charact.* **2018**, *142*, 602–612. [CrossRef]
38. Farkoosh, A.R.; Javidani, M.; Hoseini, M.; Larouche, D.; Pekguleryuz, M. Phase formation in as-solidified and heat-treated Al-Si-Cu-Mg-Ni alloys: Thermodynamic assessment and experimental investigation for alloy design. *J. Alloys Compd.* **2013**, *551*, 596–606. [CrossRef]


**Disclaimer/Publisher's Note:** The statements, opinions and data contained in all publications are solely those of the individual author(s) and contributor(s) and not of MDPI and/or the editor(s). MDPI and/or the editor(s) disclaim responsibility for any injury to people or property resulting from any ideas, methods, instructions or products referred to in the content.